Jinliang Xu[1]
State Key Laboratory of Alternate Electrical Power
System With Renewable Energy Sources,
North China Electric Power University,
Beijing 102206, China
e-mail: xjl@ncepu.edu.cn

Cheng Tang
The Beijing Key Laboratory of
Multiphase Flow and Heat Transfer,
North China Electric Power University,
Beijing 102206, China

Yongpan Cheng
The Beijing Key Laboratory of
Multiphase Flow and Heat Transfer,
North China Electric Power University,
Beijing 102206, China

Zijin Li
The Beijing Key Laboratory of
Multiphase Flow and Heat Transfer,
North China Electric Power University,
Beijing 102206, China

Hui Cao
The Beijing Key Laboratory of
Multiphase Flow and Heat Transfer,
North China Electric Power University,
Beijing 102206, China

Xiongjiang Yu
The Beijing Key Laboratory of
Multiphase Flow and Heat Transfer,
North China Electric Power University,
Beijing 102206, China

Yuzhang Li
The Beijing Key Laboratory of
Multiphase Flow and Heat Transfer,
North China Electric Power University,
Beijing 102206, China

Yanjuan Wang
The Beijing Key Laboratory of
Multiphase Flow and Heat Transfer,
North China Electric Power University,
Beijing 102206, China

Design, Construction, and Characterization of an Adjustable 70 kW High-Flux Solar Simulator

The design, construction, and characterization of a solar simulator are reported. The solar simulator consists of an optical system, a power source system, an air cooling system, a control system, and a calibration system. Seven xenon short-arc lamps were used, each consuming 10 kW electricity. The lamps were aligned at the reflector ellipsoidal axis. The stochastic Monte Carlo method analyzed the interactions between light rays and reflector surfaces as well as participating media. The seven lamps have a common focal plane. The focal plane diameters can be changed in the range of 60–120 mm with the lamp module traveling the distance in a range of 0–300 mm. The calibration process established a linear relationship between irradiant fluxes and grayscale values. The measures to reduce irradiant flux error and fluctuations were described. The irradiant flux distribution can be changed by varying the power capacities and/or moving the focal plane locations. The peak fluxes are 1.92, 3.16, and 3.91 MW/m^2 for 25%, 50%, and 75% of the full power capacity. The peak flux and temperature exceed 4 MW/m^2 and 2300 K, respectively, for the full power capacity. A 8 cm thick refractory brick can be melt in 2 min with the melting temperature of about 2300 K when the solar simulator is operating at 70% of the maximum power capacity. [DOI: 10.1115/1.4033498]

Keywords: solar simulator, solar energy, radiative flux, optical system, focal plane

1 Introduction

Solar energy is clean and abundant on earth. There are no pollutant emissions during its utilization. The solar energy reaching the earth in 1 hr is more than the annually consumed fossil fuel energy worldwide [1]. However, natural solar irradiation is intermittent with low intensity. For example, irradiance from the outer space is only about 1.36 kW/m^2. Solar energy is also affected by climate and geographic location, preventing the large-scale utilization. One way to overcome these issues is to use concentrating solar power (CSP) for high-temperature processes. In order to perform studies on CSP, an indoor solar simulator is necessary to provide a controllable and adjustable radiation flux for experiments. Table 1 summarized some solar simulators built by various researchers in the literature. The power consumption, spot size, and peak and average radiative fluxes are shown in Table 1.

For the solar simulator, the light concentrating system has significant influence on radiative fluxes on the focal plane, especially for the multilamps system. In order to achieve high solar simulator performance, precise fabrication and assembly are necessary. Manual adjustment is time-consuming and risky due to high solar radiation at high temperatures.

Because the investigations on solar energy under the nature environment have many limitations, the development of solar simulators is necessary. Even though there are some solar simulators built worldwide, these solar simulators need to be further improved. For instance, some solar simulators cannot be fully controlled with their radiative fluxes, temperatures, and power

---

capacities. Some solar simulators are not well cooled. Thus, they cannot be continuously operated. Or, the parameters of the solar simulators have narrowed ranges. Some experiments related to the solar energy are difficult to be performed with these solar simulators.

This paper is a long-term project related to the solar energy studies in China. The developed solar simulator provides a comprehensive facility for the solar energy studies. These studies include the research and development on high-flux solar receivers, solar reactors, solar energy storages, etc. In order to do so, the solar simulator should have wide parameter ranges, such as radiative fluxes, temperatures, and spot sizes. It should be well controlled and cooled for the continuous operation.

Radiative fluxes should be continuously changed instead of stepwise change by operating specific number of lamps. In our present solar simulator design, this objective was achieved by adjusting the spot diameter at the focal plane from 6 to 12 cm. Furthermore, the recorded image is severely distorted if the CCD camera axis is not perpendicular to the focal plane. The image distortion was corrected for the precise radiative flux measurement. The parameters of our solar simulator are as follows: the radiative flux on a 6 cm diameter circular target exceeds 4 MW/m^2, and the stagnation temperature reaches at least 2300 K.

In this paper, the Monte Carlo ray tracing method optimized the optical system. The analysis includes the ellipsoidal reflectors, the lamp arrangement in reflectors, and the lamp assembly to achieve a focal plane. The solar simulator performance was characterized to prove that the designed objectives were achieved. The radiative flux on the focal plane was measured. The solar simulator provides an ideal platform for high-temperature thermal or thermal–chemical studies for solar energy applications. The solar simulator was built in North China Electric Power University, Beijing, China.

2 The Development of the Solar Simulator

2.1 The Solar Simulator Layout. The solar simulator has a comprehensive design and construction. It includes the optical system, power system, air cooling system, calibration and measurement system, and control system. Seven xenon short-arc lamps were assembled to form the optical system. Each lamp consumes 10 kW electricity, maximally. A lamp and its reflector form a lamp/reflector module. It is noted that for each lamp/reflector module, the lamp can be moved relative to its reflector. The seven lamps share a common focal plane. The spot size for each lamp/reflector and the overlapping spot size of the seven lamps on the focal plane can be adjusted by the seven independent stepping motor. Seven xenon arc lamps were adopted with hexagonal arrangement (see Fig. 1(a)). Figure 1(b) shows the side view of the solar simulator, with lamps arranged in each corresponding guide rail driven by corresponding stepping motor.

The lamp/reflector module needs air cooling to maintain acceptable temperature. Attention was paid to the air quality and flow rate. The fresh air was initially dried to remove the water-vapor in the air, preventing lamps from explosion. The humid air contains small water droplets. When the air stream containing small drop particles attach a hot surface, the evaporation heat
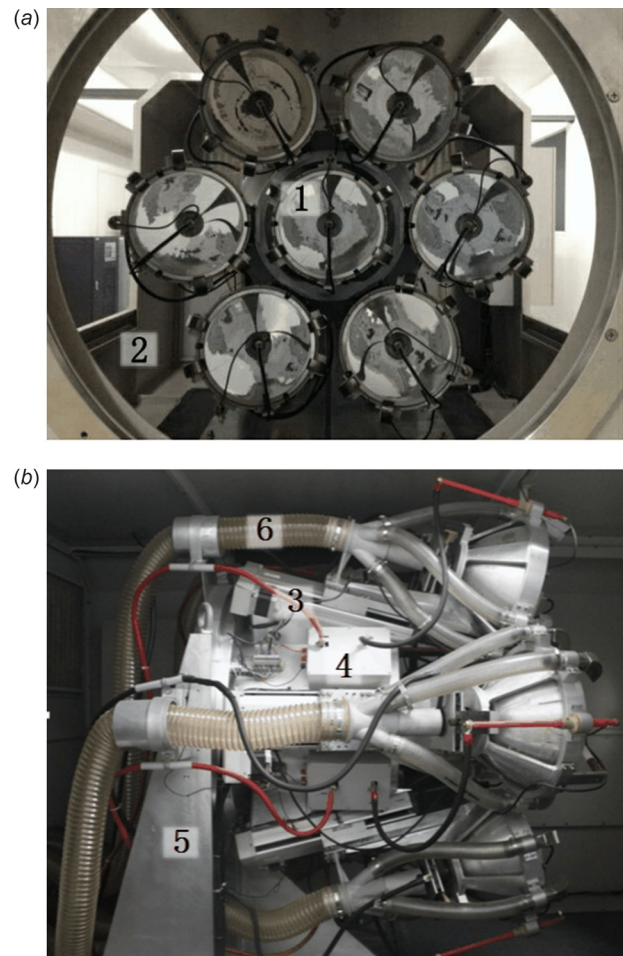

Fig. 1 The assembled group of seven xenon arc lamps: (a) front view and (b) side view—1: xenon lamp with reflector, 2: experimental cabin, 3: stepping motor, 4: trigger of xenon lamp, 5: permanent seat, and 6: duct of cooling air

transfer takes place. Because the hot surface has much higher temperature than the water droplet, the evaporation heat transfer is an explosion process. It is possible to cause damage to the facility. Thus, dry air is needed to prevent the facility from damage.

During the solar simulator operation, the air flow rate was carefully adjusted to maintain long-term operation of the solar simulator. The air flow rate was provided by a centrifugal fan. After the air entered the engineering room of the solar simulator, the total flow rate was divided into seven air streams. Each air stream flows through the corresponding lamp/reflector module. The air was finally discharged to the outdoor environment. The air temperature near the reflector surface was limited by 150 °C. Seven power sources acted as the electricity suppliers to drive the xenon lamps. Each power source drives its corresponding lamp. When the loss of electricity occurs, the cooling system and control system do not
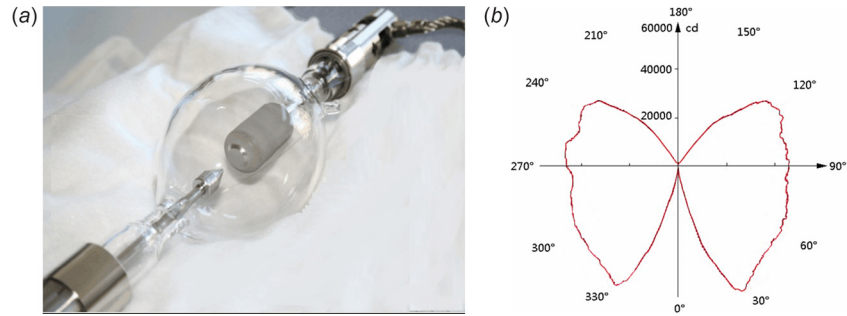
Fig. 2 (*a*) **Photo of the xenon short-arc lamp (OSRAM XBO**® **10000 W/HS OFR) and** (*b*) **luminous intensity distribution curve (the curve is provided by the OSRAM Corporation, Munich, Germany)**

work immediately, but the lamp and reflector are still on the high temperature. Thus, an uninterruptible power system (UPS) is needed to provide the sustainable electricity to ensure the safety of the solar simulator.

The control system is important for the system operation and safety. Various sensors and instruments were installed for the solar simulator. The focal plane diameter is one of the important control parameters. Initially, a desired focal plane size is set for the control system. The control system utilized the relationship between the focal plane diameter and the guide rail displacement to adjust the lamp/reflector axial position. Thus, a desired focal plane diameter is reached.

The operation of xenon lamps needs the trigger and power control system. Once the lamps are triggered to shine, the camera in the engineering room records the images and the image signal is sent to the display screen of the control system. Thus, the operation of xenon lamps was visualized. The current flowing through xenon lamps was collected and controlled to maintain a suitable power capacity for the solar simulator. In the case of loss of the external power grid (electricity), the lamps are off but the temperatures are still high. The air flow rate is continuously supplied driven by the UPS power source.

2.2 Selection of Lamp. Both xenon arc lamps and metal halide lamps can emit spectrum distribution mostly close to sunlight. The size of light sources from metal halide lamps is larger than that of xenon arc lamps. The ellipsoidal reflector focuses the light emitted from one focal point to another focal point. The distance between the light arriving point and the target focal point is related to the distance between the emission point and the initial focal point. The lamps are not ideal point light sources. Thus, the lamps are represented by the cylindrical illuminant bodies. Compared with ideal point light source, the rays launched from the cylindrical body surface travel shorter to the second foci. Thus, high-radiative flux can be reached by smaller light source. There are longer or shorter xenon lamps. The long-arc lamps have high power with water cooling, but the transfer efficiency is low. Alternatively, xenon short-arc lamps are more close to point light source, the start-up time is short. Thus, the short-arc lamp (OSRAM XBO® 10,000 W/HS OFR) is used in our solar simulator.

Both single lamp and multilamps can emit high-flux radiation. The single-lamp simulator has simple concentrating system with high reliability. The high-power lamp needs cooling to ensure its safe operation. For some solar simulators with water-cooling system, part of the emitted rays are absorbed and scattered by the cooling water. This would lower the radiative fluxes reached at the focal plane. Instead, we used the air cooling system to avoid the flux decay. High temperature may also cause cooling system problem. This drawback can be overcome by multilamps. The multilamps simulator uses air cooling instead of water cooling. The light ray is not disturbed. The radiation flux can be easily

adjusted by changing the number of operating lamps. For example, the multilamps simulator has advantages over the single-lamp simulator, even though the concentrating system is a little bit complicated. Here, we used the multilamps simulator.

2.3 Arrangement of Lamps in Reflectors. Figure 2(*a*) shows the short-arc xenon lamp. Both cathode and anode are in a spherical quartz bulb and separated by an electrode gap. According to the short xenon arc lamp characteristic (OSRAM XBO® 10,000 W/HS OFR), the arc can be considered as a cylinder with a 2.5 mm diameter and a 3 mm length. Most of the emitted rays are radiated from this cylinder region. Figure 2(*b*) shows luminous intensity distribution (provided by OSRAM Corporation, Munich, Germany) of the short xenon arc lamp. The butterfly distribution is due to the distinct geometrical and optical characteristics of the lamp. The coordinate origin is located at the cathode point. The vertical axis ($\theta = 0$ deg and 180 deg) stands for the axis between anode and cathode. It is found that the emitted irradiance along the anode–cathode direction is negligible. The light source can be assumed to emit from a cylinder excluding both ends. We put a refractory brick on the spot location of the focal plane of the solar simulator (see Fig. 3). When the solar simulator is operating at 70% of the maximum power capacity, the brick is being melted in 2 min, noting that the melting temperature of the brick is about 2300 K.

Figures 4(*a*) and 4(*b*) show that the axis of xenon arc lamp is located either perpendicular to or aligned at the reflector ellipsoidal axis. A secondary sphere mirror is needed to reflect emitted rays to the reflector for perpendicular arrangement (see Fig. 4(*a*)). It is noted that the reflector has a hole in its apex. The hole is used to pass through the air flow rate to ensure the successful cooling of the lamp/reflector module. The Monte Carlo ray tracing method in TRACEPRO 7.0 [10] was applied to evaluate the radiative

Fig. 3 A refractory brick is being melt by the solar simulator, the melting temperature of the brick is about 2300 K
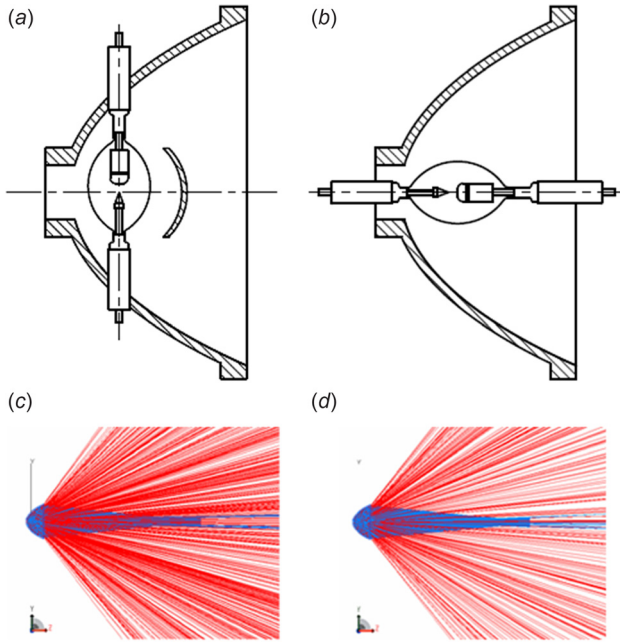
Fig. 4 The xenon arc lamp in the reflector: (a) perpendicular arrangement, (b) aligned arrangement, (c) reflected (concentrated to the focal plane) and nonreflected rays (dispersed to the environment) vector

transport for solar simulator. Vacuum medium is used as the participating media for the Monte Carlo simulation. The radiative energy is divided into a number of discrete energy rays. The stochastic Monte Carlo method determines the initial location, direction, and wavelength of a ray. Thus, the ray paths are tracked. The interactions between light rays and reflector surfaces as well as participating media are simulated. The radiative energy at a location is computed by integrating the number of rays by the Monte Carlo simulation. The transfer efficiency η is defined as the fraction of radiation leaving the sources divided by that reaches the target, which can be written as

$$\eta = \sum_{j=1}^{N} q_j'' A_j \Big/ \sum_{j=1}^{M} q_i'' A_i \tag{1}$$

where M, N, q_i'', and q'' are the number of radiation sources, the number of discrete elements on the target, the radiative flux leaving the ith source, and the radiative flux intercepted by the jth discrete target element.

Figures 4(c) and 4(d) show the ray paths for perpendicular and aligned positioned short arcs in reflectors, respectively. We note that concentrated and dispersed vectors are nonreflected rays and reflected rays, respectively. The radiative flux distributions are compared between perpendicular and aligned positioned arc lamps in reflectors. For the perpendicular aligned arc lamp, more rays are emitted to ambient from the xenon lamps without reaching the reflector, yielding weak radiative fluxes. The perpendicular positioned arc lamp has poor symmetric irradiance distribution with two peak values in the irradiance distribution along x-axis. This mode has a peak radiative flux of 1900 kW/m² and a transfer efficiency of 0.71. The aligned arrangement has symmetrical radiative flux distribution with uniform radial flux distribution. The radiative energy is focused on a 20 mm circular region with a peak radiative flux of 2600 kW/m² and a transfer efficiency of 0.80. Hence, the aligned arranged arc lamp is superior to the perpendicular arranged arc lamp. Our solar simulator used the aligned positioned arc lamp scheme.

2.4 The Reflector Optimization. The reflector has ellipsoidal shape. The light rays emitted from one focal point are concentrated on another focal point. Figure 5(a) shows the seven xenon arc lamps with the hexagonal arrangement. All the seven lamps concentrate the emitted rays on a common focal point F_2, which is on a sphere having a diameter of $4c$, c is called the focal length (see Fig. 5(b) and 5(c)). The sphere center is located at the first focal point F_1. In Figs. 5(b) and 5(c), the truncation angle is α, the truncation diameter is D, and the inclination angle is θ. Specified by the manufacture limit, D is equal or less than 400 mm and θ is equal or less than 15 deg. Figure 5(c) shows the cross section of ellipsoidal revolution for reflector. The ellipse equation is

$$\frac{1}{a^2}\left(x^2 + \frac{y^2}{1-e^2}\right) = 1 \tag{2}$$

where $e = c/a$ is the eccentricity.

Both the focal length c and major axis length a depend on D, α, and θ. The eccentricity e is only dependent on α and θ and independent on D. The parameter relationships are

$$c = \frac{D}{4}\left(\frac{1}{\tan\alpha} + \frac{1}{\tan\frac{\theta}{2}}\right) \tag{3}$$

$$a = \frac{D}{4}\left(\frac{1}{\sin\alpha} + \frac{1}{\sin\frac{\theta}{2}}\right) \tag{4}$$

$$e = \frac{c}{a} = \cos\alpha\cos\frac{\theta}{2}\cdot\frac{\tan\alpha + \tan\frac{\theta}{2}}{\sin\alpha + \sin\frac{\theta}{2}} \tag{5}$$

The TRACEPRO software simulated the transfer efficiencies varying with the eccentricities e. Thus, the e value is obtained at which the transfer efficiency is maximum. The truncation angle (α) is obtained by Eq. (5) with known inclination angle θ. The maximum D of 400 mm is limited by the fabrication limit of the optical facility in China. Figure 6 shows the effects of D and α on η, showing no effect of D on η. But η is sharply increased when α is increased from 30 deg to 60 deg, followed by a slight decrease when α exceeds 60 deg (see Fig. 6(b)). Two mechanisms cause the loss of radiative power: by reflection of off-focal point radiation and/or by the escaped radiation due to truncation. For an ideal point light source at the focal point, all the emitted rays are concentrated on another focal point, which is independent on the truncation angle. A practical lamp cannot be a point source. The
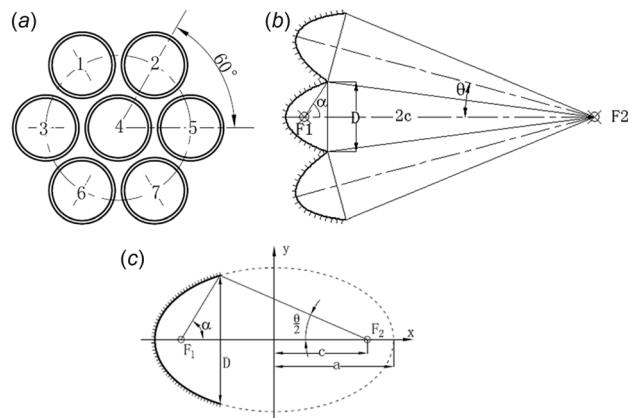

Fig. 5 Optical layout of lamps and reflectors: (a) front view, (b) side view, and (c) the ellipse coordinate system
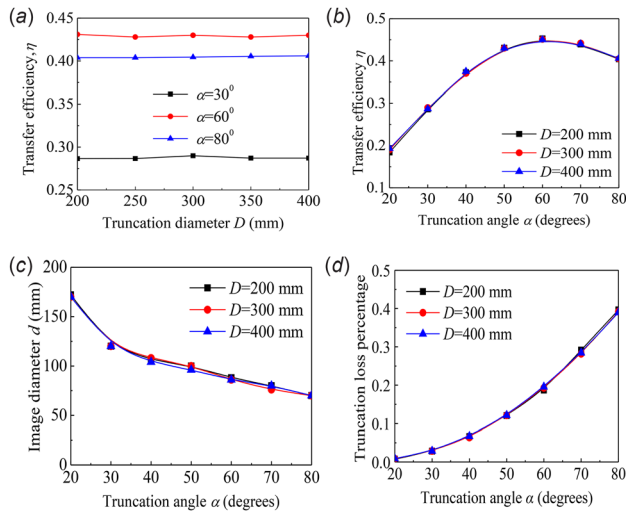
Fig. 6 Effects of truncation diameters and angles on the optical performance

distance between the ray emission point and the focal point determines the distance between the ray arriving point and the target focal point, which is dependent on truncation angles. The eccentricity e increases with the decrease of the truncation angle α, indicating the increased deviating degree of ellipsoid from sphere. This effect enlarges the lamp images with the decrease of α (see Fig. 6(c)). The radiative power loss is enhanced if the image is larger than the target focal area.

One shall remember that reflectors are actually the truncated ellipsoids. Part of radiative power from lamps is emitted to ambient without reflection. Such part of energy cannot reach the focal target. The truncation area of ellipsoid is increased with the increase of truncation angle α to yield larger radiation loss (see Fig. 6(d)). The transfer efficiency η reaches maximum due to the lowest off-focal point radiation and escaped radiation which are simulated in TRACEPRO at $\alpha = 60$ deg, having $a = 1180$ mm (major axis length), $c = 1025$ mm (focal length), and $D = 400$ mm (truncation diameter, D must be equal or less than 400 mm because the limitation of the optical reflector machining technology in China). These parameters are used for our solar simulator.

In addition to the front truncation of reflectors, the back truncation eases the installation and air cooling of lamps. The back truncation diameter was set as 62.5 mm. Cooling air was injected to the xenon lamps through the back truncation section and four front truncation nozzles. The minimum air velocity was 10 m/s to ensure the safe operation of xenon lamps. The reflectors were made of light aluminum alloy. The reflector surface was polished and uniformly coated with a thickness of 70 μm nickel. Finally, the surface was covered with a reflective layer of aluminum coating with an oxidation-preventing layer applied on top of it. The reflection efficiency was up to 94%. Figure 7 shows the reflector before and after surface treatment. There is an oxidation-preventing layer on the aluminum coating surface. The solar simulator system needs careful maintenance. For daily maintenance,
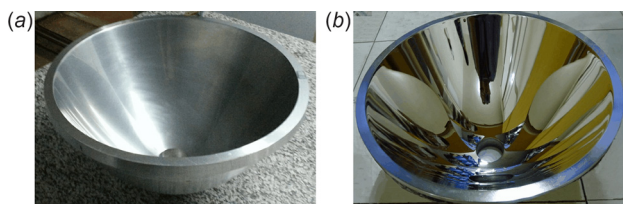
the extremely dry working environment is ensured by an air dehumidifier. The dry condition significantly prevents the coating surface from oxidation.

2.5 Assembly of Lamps. The seven xenon lamps are assembled in a hexagonal form. Two ways can change the focal plane size, either by changing the inclination angle of reflectors or by changing the distance between reflectors and focal point. For the inclination angle adjustment scheme, six lamps and the reflector are installed in the hexagonal frame. The seventh lamp was at the center. Because reflectors and supporting components are heavy, they must be installed vertically to ensure stability and precise adjustment. Each lamp and reflector module can rotate around the vertical axis. Their ends are connected to the nut through the connection bar. When the nut rotates around the vertical rod, it pulls or pushes the lamp/reflector module to rotate against the vertical axis. Thus, the inclination angle of lamps with respect to the focal plane is changed.

This paper used the second scheme (see Fig. 8). The seven lamps have a common and fixed focal plane. Each module consisting of a lamp and its reflector have independent mechanical and controlling system. The location of each module can be precisely adjusted by a stepping motor. The distance between module and focal plane can be changed driven by the stepping motor. Thus, the focal plane size is changed. The inclination angle for each of the surrounding six lamp modules with respect to the central lamp module is fixed as 15 deg. Figure 8(a) shows the lamp module group. Figure 8(b) shows the guide rail to support the lamp module.

Figure 9 shows effect of inclination angles on focal plane location. At the inclination angle of 15 deg, the focal plane is located at position I with the focal length of 2050 mm, where the focal
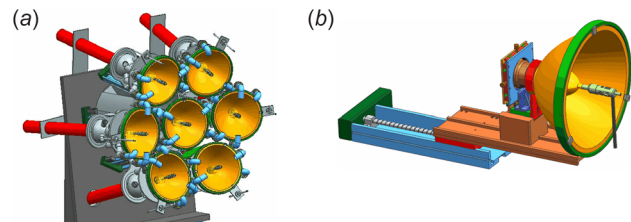

Fig. 8 (a) The spot size on the focal plane was changed by the axial location of the lamp/reflector module and (b) each lamp/reflector module was positioned in a guide rail driven by a stepping motor
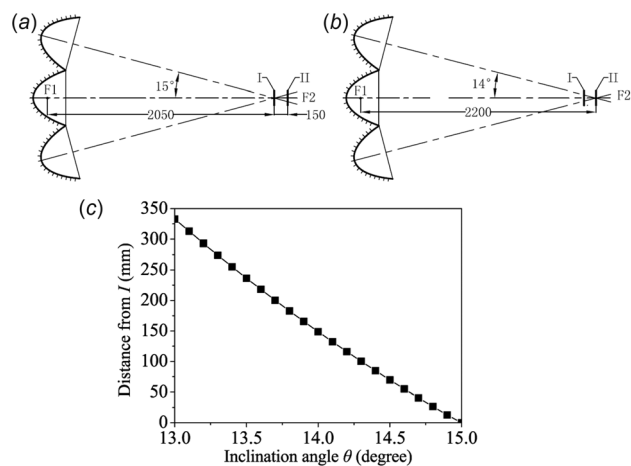

Fig. 9 Focal plane locations dependent on inclination angles: (a) focal plane located at plane I at $\theta = 15$ deg, (b) focal plane located at plane II at $\theta = 14$ deg, and (c) the deviation distance from focal plane I versus inclination angle θ

Fig. 7 (a) The photo of a reflector before the surface treatment and (b) the photo of a reflector after the surface treatment

length is the distance between the focal points of F_1 and F_2. If the inclination angle of reflectors is reduced to 14 deg, the focal plane will be moved to the location II, which is 150 mm away from the location I, indicating that the focal plane location is sensitive to the inclination angles. This study used the second scheme to adjust the spot size. The spot diameter will be changed from 60 to 120 mm with the lamp/reflector module traveling the distance in a range of 0–300 mm.

3   Characterization of the Solar Simulator

A high-radiative flux meter (Gardon type, Medthermo 64 series) was used as a sensor. The manufacturer provided the calibration curve of radiative flux versus the output voltages. The measurement covered the spectral range from 300 nm to 5000 nm. The calibration procedure compared the measured radiative fluxes with the grayscale values obtained by a CCD camera (photon counter). In such a way, the relationship between the radiative fluxes and the grayscale values is obtained.

Radiative flux distribution on the focal plane is obtained by the linear relationship between radiative flux and grayscale on the diffuse reflection surface. The CCD camera captures the grayscale distribution on the whole surface. The radiative flux meter measures the radiative flux on specific locations. The radiative flux on any point is

$$I = a' \times G \tag{6}$$

where I is the radiative flux, G is the grayscale value, and a' is the linear coefficient, which should be calibrated. It is noted that, even though a 8-bit camera is used, a lot of images are summed up to increase the effective bits for the image file processing.

The radiative flux meter has a copper shell and a sapphire window. It is water cooled to keep a temperature less than 25 °C. The radiative flux has a linear relationship with the voltage as $I = 0.984 V$, where I has a unit of MW/m². The Lambert plate has a rectangular size of 400 mm × 300 mm. It is an aluminum plate coated with a uniform aluminum oxide layer. The CCD camera takes pictures with the grayscale range of 0–255. The data-acquisition system collects the measured voltage signal. A three-dimensional guide rail system supports the Lambert plate and the radiative flux meter to ensure the plate exactly on the focal plane.

The calibration involved four steps: (1) Radiative fluxes were measured on specific number of points on the Lambert plate. (2) The CCD camera measured the grayscale values on the whole focal plane. (3) The conversion between natural coordinate and project coordinate was performed. Thus, the real grayscale values on the focal plane were obtained. A link between the grayscale value and radiative flux was established. (4) A linear correlation between radiative fluxes and grayscale values was achieved. Thus, the radiative fluxes on the whole focal plane can be calculated based on the calibration.

The radiative fluxes oscillate after the trigger of the xenon arc lamps. The oscillation amplitude is weakened versus time. Two mechanisms cause the oscillation of radiative fluxes. The xenon gas can only be triggered after a specific time of electric discharge. Besides, the power source also causes the oscillation of the radiative fluxes. The power source driving the xenon lamps can be characterized by the filtering quality. It is noted that the xenon lamps are driven by the direct current (DC) voltage. The term of "filtering" refers to smoothing the alternating current component from the power source. The filtering quality is defined as

$$S = \frac{V_{max} - V_{min}}{2V_d} \tag{7}$$

where V_{max} is the maximum input voltage, V_{min} is the minimum input voltage, and V_d is the average voltage output (direct current). The irradiance fluctuation ratio of the radiative fluxes is defined as

$$\sigma = \frac{I - \bar{I}}{\bar{I}} \times 100\%, \quad \bar{I} = \frac{1}{N}\sum_{i=1}^{N} I_i \tag{8}$$

where I is a measured radiative flux, $\bar{I}$ is the average radiative flux in a specific period of time, and N is the sampling number.

Figure 10 shows irradiance fluctuation ratio versus time for 50% of the full power capacity. The data were shown during the period of 120–144 s and 320–342 s after triggering of the xenon lamps. The data sampling rate is 1 Hz. It is shown that the fluctuations are increasing for the first time period. However, the radiative fluxes became quite stable after 320 s of the lamp triggering. Most of fluctuation data points have 0.2–0.3% oscillation, showing quite stable radiative fluxes. It is noted that the transition time from the unstable to stable signal output is decreased with the increase of the power capacity.

An important step for measurements is to eliminate the dark voltage, which can be obtained with the optical window of the radiative flux meter in the dark condition (without light irradiating). After eliminating the dark voltage, the radiative flux is rewritten as

$$I = a'(V_0 - V') \tag{9}$$

where V_0 is the output voltage of the radiative flux meter, and V' is the measured dark voltage.

A high-accuracy measurement of radiative flux needs perpendicular irradiating of light rays on the radiative flux meter. The solar simulator cannot emit perfectly parallel light rays. Some part of the rays are not irradiating on the photosensitive element of the radiative flux meter, but shining on the side walls of the radiative flux meter. This nonperpendicular irradiating effect lowers the radiative fluxes. Besides, the sapphire window of the radiative flux meter has specific reflectivity and absorptivity values. The radiative flux should be calibrated by using laser rays with known radiative flux. The calibration result yields the comprehensive absorptivity of 0.92. Thus, the radiative flux is obtained by the measured value multiplying by a factor of 1.086.

This study changes the DC current flowing through the xenon lamps to adjust the power capacity and radiative fluxes on the focal plane. Figure 11 shows the finally obtained radiative flux distribution on the focal plane (Lambert plate). It is shown that the center of the light spot is stabilized for each power capacity. The radiative fluxes are continuous and uniform versus the circumference angles, showing the perfect symmetrical characteristic in circumference angle direction.

The peak fluxes are 1.92, 3.16, and 3.91 MW/m² for 25%, 50%, and 75% of the full power capacity, respectively. The slopes of the peak fluxes with respect to the power capacities are decreased with the increase of the power capacities. The peak flux at the full power capacity exceeds 4 MW/m². The solar simulator limits the power capacity of 90% for practical applications [11]. The solar simulator for the solar receiver application can be found in Ref. [12]. The nonlinear relationship between the radiative fluxes and the power capacities is due to the decreased electro-optical conversion efficiency at high-power capacities. The major radiative
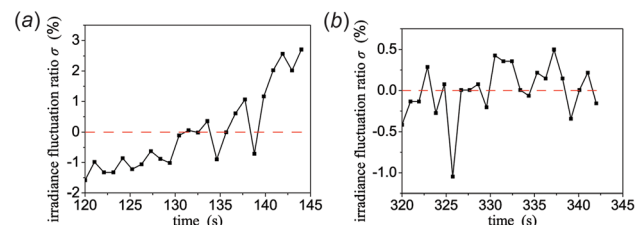

Fig. 10   The irradiance fluctuations ratios at 50% of the full power capacity: (a) oscillation in the period of 120–144 s and (b) oscillation in the period of 320–342 s
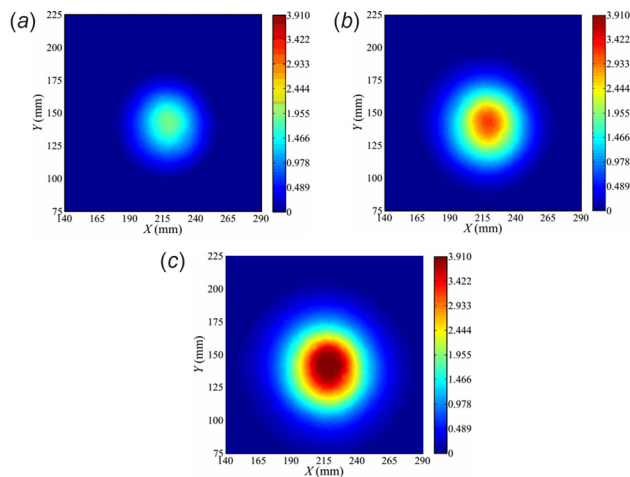
Fig. 11   Radiative flux distributions in MW/m^2: (*a*) at 25% of the maximum xenon arc lamp power capacity, (*b*) at 50% of the maximum xenon arc lamp power capacity, (*c*) at 75% of the maximum xenon arc lamp power capacity

energy is focused on the 60–80 mm circular region. The light focusing region is slightly enlarged by increasing the power capacities.

Figure 11 shows that the light spot area and the ultrahigh radiative flux area are enlarged by increasing the power capacities. The developed solar simulator has ultrahigh concentration ratio. The radiative flux distribution and its area can be changed by varying the power capacities and/or moving the focal plane locations, satisfying different experiment requirements.

4   Conclusions

The solar simulator used seven independent xenon arc lamps as the light source. Each lamp consumes 10 kW electricity and has its own reflector. The emitted rays are reflected to a common focal plane. The seven guide rails adjust the distance between lamp and focal plane, simultaneously or independently. The adjustment resolution attains 0.1 mm.

The radiative fluxes can be changed by varying the power capacity applied on lamps and/or mechanical driving system. The comprehensive control platform monitors and operates the solar simulator. The seven xenon arc lamps and their mechanical driving system are enclosed in a warehouse for security purpose. The pressure and temperature inside the warehouse are monitored and controlled. The air cooling system ensures the major components to operate at limited temperature level. A set of infrared ray sensors measured the temperatures of the xenon lamps to ensure their safety. For the safety consideration, the temperatures of the electrodes and reflectors should be monitored. The electrode's temperature should be less than 450 K and the reflector's temperature should be smaller than 423 K, based on the requirement. The UPS ensures the continuous electricity supply to the solar simulator, further ensuring the system safety after the sharp power loss of the external power grid.

The solar simulator consumes maximum 70 kW electricity. The radiative energy on the focal plane is about 20 kW to indicate an overall electro-optical conversion efficiency of about 29%. The radiative energy is mostly focused on a 60–80 mm diameter circular target. The peak flux reaches 4 MW/m^2. The solar simulator can melt a refractory brick in 1 min. The brick has a melting temperature of 2000 K. In summary, the solar simulator simulates the radiation characteristics of highly concentrating solar systems and serves as an experimental platform for investigating the thermochemical processing of solar fuels and for testing advanced high-temperature materials.

References

[1] Steinfeld, A., and Meier, A., 2004, "Solar Fuels and Materials," *Encyclopedia of Energy*, Vol. 15, C. Cleveland, ed., Elsevier, Amsterdam, The Netherlands.
[2] Kuhn, P., and Hunt, A., 1991, "A New Solar Simulator to Study High Temperature Solid-State Reactions With Highly Concentrated Radiation," Sol. Energy Mater., **24**(1–2), pp. 742–750.
[3] Hirsch, D., Zedtwitz, P. V., Osinga, T., Kinamore, J., and Steinfeld, A., 2003, "A New 75 kW High-Flux Solar Simulator for High-Temperature Thermal and Thermochemical Research," ASME J. Sol. Energy Eng., **125**(1), pp. 117–120.
[4] Petrasch, J., Coray, P., Meier, A., Brack, M., Häberling, P., Wuillemin, D., and Steinfeld, A., 2007, "A Novel 50 kW 11,000 Suns High-Flux Solar Simulator," ASME J. Sol. Energy Eng., **129**(4), pp. 405–411.
[5] Dibowski, H. G., 2013, "High-Flux Solar Furnace and Xenon-High-Flux Solar Simulator," DLR–Institute of Solar Research, Köln, Germany
[6] Krueger, K. R., Davidson, J. H., and Lipinski, W., 2011, "Design of a New 45 kWe High-Flux Solar Simulator for High-Temperature Solar Thermal and Thermochemical Research," ASME J. Sol. Energy Eng., **133**(1), p. 011013.
[7] Krueger, K. R., Lipinski, W., and Davidson, J. H., 2013, "Operational Performance of the University of Minnesota 45 kWe High-Flux Solar Simulator," ASME J. Sol. Energy Eng., **135**(4), p. 044501.
[8] Sarwar, J., Georgakis, G., LaChance, R., and Ozalp, N., 2014, "Description and Characterization of an Adjustable Flux Solar Simulator for Solar Thermal, Thermochemical and Photovoltaic Applications," Sol. Energy, **100**(2), pp. 179–194.
[9] Codd, D. S., Carlson, A., Rees, J., and Slocum, A. H., 2010, "A Low Cost High Flux Solar Simulator," Sol. Energy, **84**(12), pp. 2202–2212.
[10] Lambda Research, 2011, "Trace Pro 7.0," Lambda Research Corp., Littleton, MA.
[11] Li, Q., 2011, "Preliminary Study on Light Source of High Irradiance Solar Simulator," Master's thesis, University of Science and Technology of China, Hefei, China.
[12] Bader, R., Barbato, M., Pedretti, A., and Steinfeld, A., 2010, "An Air-Based Cavity Receiver for Solar Trough Concentrators," ASME J. Sol. Energy Eng., **132**(3), p. 031017.